High Resolution T-O-F Positron Emission Tomograph

I. 18. High Resolution T-O-F Positron Emission Tomograph

Ishii K., Orihara H., Matsuzawa T., Binkley D. M.** and Nutt R.***

Cyclotron and Radioisotope Center, Tohoku University
*Research Institute for Tuberculosis and Cancer, Tohoku University**
*CTI PET Systems, Inc., 810 Innovation Drive, Knoxville, Tennessee 37932, USA***

1. Introduction

In the case of a conventional PET[1-3], the images of a low activity region close to a high activity region are reconstructed including the noise induced by the statistical errors of positron events in the high activity region. This difficulty may be reduced however by using the time-of-flight location on coincidence lines ($x = (t_2-t_1)\ C/2$, where x is the distance from the middle point between detectors 1 and 2 which face each other, $t_{1(2)}$ is the time of flight of γ-ray from the position of annihilation to the detector 1(2) and C the light velocity.) The use of a fast decay component of light from a BaF_2[7] or CsF scintillator enables such a coincident measurement, while it is impossible for BGO and NaI scintillators which are used in a conventional PET. The positron emission tomograph based on this idea is called a time-of-flight (TOF) PET which provides high quality images with a good S/N ratio.[5,6] The reduced image noise of TOF·PET[8-11] will permit us to find delicate or fine changes in metabolism in the presence of a strong background. For this reason, the TOF·PET was constructed.

2. System Description

The TOF·PET consists of a gantry, data acquisition system and data processing system which are shown in Fig. 1.

[1] Gantry

The gantry currently consists of one detector ring with 16 detector buckets each having 16 BaF_2 scintillation detectors. It is possible to upgrade the present gantry from one ring to multiple rings. The total number of detectors is 256 per ring and the diameter of detector ring, that is, the distance from a surface of detector to that of an opposite side is 102 cm.

Lead plates between detectors are used to define a detector width and also shield them from scattered γ-rays. The BaF_2 crystal has a polyhedron shape shown in Fig. 2 and is covered with a teflon tape and TiO_2 powder which reflects the photons of the fast decay component well.[12] The photomultipliers, with a quartz window of 10 mm in diameter (Hamamatsu R2496), are coupled to BaF_2 crystals with a transparent liquid silicone rubber compound (RTV).

Anode signals of the photomultipliers are fed to a newly designed CFD[14] which produces fast timing signals. Accumulating only the photopeak is desired for reduction of background induced by scattered γ-rays, however, a threshold level of 250 keV was adopted to improve detector efficiency. The time when a γ-ray arrives at a photomultiplier is recorded by a time digital converter (TDC) using system clock pulses of 16 nsec and 256 nsec in periods. Arriving time and detector numbers are transferred from detector buckets to a ring receiver in the data acquisition system.

A large patient opening (90 cm) is used to measure simultaneous patient emission and transmission source using the T-O-F technique. The T-O-F technique permits a separation between emission and transmission events. The gantry can be wobbled with an orbit of 12.4 mm in diameter for high resolution studies. It is also possible to tilt (±30°) and rotate the gantry.

[2] Data Acquisition System

The ring receiver, coincidence processor[15] and real time sorter (RTS) of the PT931[16] conventional PET are used in the data acquisition system of the present TOF-PET. The coincidence processor, however, is modified to record T-O-F information and the RTS[17] is supplemented by a T-O-F formatter. Every 256 nanoseconds, the ring receiver accepts event data and transfers to the T-O-F coincidence processor which searches a coincidence pair within a time window (12 nsec) and encodes them. 48 line-of-responses (LORs) are adopted for obtaining a field-of-view (FOV) with 56 cm diameter. The RTS calculates a detector position (d), view of angle (θ) and time of flight from the center of gantry (t) by detector Numbers (N_1 and N_2) and arriving time (t_1 and t_2) of a coincident event, and forms a three dimensional sinogram $E(d,\theta,t)$ into VME solid state memory (128 MB). The T-O-F formatter discriminates between $t = t_1 - t_2$ and $t_2 - t_1$ according to a geometric condition of N_1 and N_2.

[3] Data Processing System

Three dimensional sinograms $E(d,\theta,t)$, sorted in solid state memory of the data acquisition system, are transferred into a data disk through DMA and rearranged into a form of $S_0(t,d,\theta)$ (described later). A minicomputer (DEC micro-VAX II) and array

processors (Analogic AP500) perform an image reconstruction with the three dimensional sinogram and a display processor (Gould/De Anza FD5000) displays it on a video monitor. The programs of operation, maintenance, image reconstruction and other software are saved on a system disk.

3. Data Acquisition and Its Structure Definition

[1] Acquisition Mode

Two acquisition modes are available for requirements of low and high spatial resolution, the stationary and wobble modes respectively.

We have 256 views of projection and 48 LORs for each view. By interpolating odd angle data into those of even angles, we can define a sinogram with 96 and 128 bins for d and θ respectively in the stationary mode.

An improvement for spatial resolution is achieved by wobbling the gantry and sampling at 4 positions. The TOF sinogram with 192 and 256 bins for d and θ respectively is defined in the wobble mode.

[2] Time Structure Definition

The present system provides 32 bins of T-O-F information as shown in Fig. 3. The bins 2-30 with 125 psec/bin (18.75 mm/bin) are used in the T-O-F sinogram $S_0(t,d,\theta)$, limiting the effective field of view to 543.75 mm. In a simultaneous measurement of emission and transmission data, events from a ring source are accumulated into bin 1 and 31 with a time window 1.75 nsec. Random coincidence events in the final bin 32 are useful for a background subtraction.

4. Time Alignment

The origin of all time axes in the TOF sinogram should be accurately adjusted on a line passing the center of gantry and perpendicular to the LORs, that is, the center locations of the LORs must be accurately adjusted. The misalignments between TOF positions will result in loss of image quality obtained by T-O-F information and also result in a distortion of the image. For this purpose, we developed a unique method using a semiring source (see Fig. 4). This method can perform the time alignment within an accuracy of $\pm$31.25 psec.

5. Image Reconstruction

After the corrections for detector efficiencies and attenuation within the patient and,

moreover, for detector positions, a convolution between the TOF sinogram $S(t,d,\theta)$ and a TOF filter function is carried out and an image is reconstructed by the method previously reported.[13] A flow chart for processing TOF image reconstruction is presented in Fig. 5.

6. Performance Characteristics

[1] Scan Mode

The TOF-PET provides static emission scan, dynamic emission scan, gated emission scan (A maximum of 160 and 40 gated acquisitions are available for stationary and wobble mode respectively.) and direct imaging scan. The direct imaging scan provides us "movie" images of 15 seconds with 0.1 sec/frame. This mode is useful to observe very fast density distribution changes in a body (for an example, motion of positron isotopes), but the spatial resolution is 3~4 cm.

[2] Spatial Resolution and Time Resolution

The ^{68}Ge needle source of stainless steel tube with an inside diameter of 1.4 mm and outside diameter of 1.8 mm was used to measure the spatial resolution. Figure 6 shows the spatial resolutions as a function of distance from the center of gantry. By the use of wobble mode, we did achieve a high resolution TOF·PET with a spatial resolution of 8 mm FWHM. The axial resolution was also measured and was 9.65 mm FWHM.

An average system resolution of 623 psec FWHM ($\frac{1}{2}\Delta T \times C$ = 9.2 cm) has been obtained within a deviation of 55 psec.

[3] Sensitivity and Uniformity

A uniformly distributed source of 21 mCi ^{18}F contained in for a 20 cm by 20 cm deep cylindrical phantom has been used to measuring sensitivity and uniformity. We obtained a sensitivity of 4,054 cps/μCi/ml with a deviation of ± 5.8 %.

[4] Image Quality

A cylindrical phantom has been measured in order to examine the improvement in image quality with the use of TOF information. The cylindrical phantom was divided into three layers of which diameters were 26 mm, 150 mm and 200 mm for center, inside and outside respectively. The central and outside regions were filled with ^{18}F activated water of 0.92 μCi/cc and 8.5 μCi/cc respectively. The inside region was filled with normal water. The measurement was done for two minutes in stationary mode. Figure 7 shows the reconstructed images. The NON-TOF image was obtained by a usual method by integrating the TOF sinogram used in the TOF image over the time axis. We can see a clear difference in image quality between them. The outside ring is well reproduced in the TOF

image, but, in the case of NON-TOF image, its image is considerably affected with the artifacts due to the central region. This result is of course an effect of the use of TOF information.

The ^{18}FDG images of a middle part of human head are shown in Fig. 8 where the ^{18}FDG solution of 8.3 mCi was injected and, after 90 minutes, data was acquired in wobble mode for thirty minutes. It is seen in comparison between them that the TOF PET reproduces positron images with high confidence: The TOF image is superior in the view of reproducing the contrast in density[9], the parts lacked in the NON-TOF image (e.g. the occipital region) can been seen and a structure of interior is well reproduced in the TOF image.

The high performance TOF-PET described here is now being used for clinical studies on tumors, cardiac disease, brain infarction, dementia etc along with the conventional PETs (PT931 and ECATII) and other CT machines (MRI and X-CT) at the Research Institute for Tuberculosis and Cancer.

References

1) Ter-Pogossian M. M. *et al.*, Radiology **114** (1975) 89 .
2) Phelps M. E., Hoffman E. J., Mullani N. A. and Ter-Pogossian M. M. , J. Nucl. Med. **16** (1975) 210.
3) Brooks R. A. and Dichiro G. , Phys. Med. Biol. **21** (1976) 689.
4) Reivich M. and Alarri A., *Positron Emission Tomography*, (Alan R. Liss, Inc., New York, 1985).
5) Soussaline F., Comar D., Allemand R., Campagnolo R., Laval M. and Vacher J., *The Metabolism of the Human Brain Studied with Positron Emission Tomography*, edited by T. Greitz *et al.* (Raven, New York, 1985), pp. 1-11.
6) Mullani N. A., Markham J., and Ter-Poggossian M. M., J. Nucl. Med. **21** (1980) 1095.
7) Laval M., Moszyski M., Allemand R., Cormoreche E., Guinet P., Odru R. and Vacher J. , Nucl. Instr. and Meth. **206** (1983) 169.
8) Ter-Pogossian M. M., Mullani N. A., Ficke D. C., Murkham S. and Snyder D. L., J. Comput. Assist. Tomogr. **5** (1981) 227.
9) Ter-Pogossian M. M., Ficke D. C., Yamamoto M., and Hood J. T., IEEE Comput. Soc. Pub. **37** (1983) 488.
10) Allemand R., Gresset C. and Vacher J., Nucl. Med. **21** (1980) 153.
11) Compagnolo R., Laval M., Moszynski M. and Soussaline F., Laboratoires Mesure, Controle et Traitement Electronique (MCTE)/82-353, 1982.
12) Ishii K., Watanuki S., Orihara H., Itoh M. and Matsuzawa T., Nucl. Instr. and Meth. A **253** (1986) 128.
13) Ishii K., Orihara H. and Matsuzawa T., Rev. Sci. Instrum. **58** (1987) 1699.
14) Binkley D. and Casey M. E., IEEE Transactions on Nuclear Science **35** (1988) 226.
15) Dent H. M., Jones W. F. and Casey M. E., IEEE Transactions on Nuclear Science **33** (1986) 556.
16) Technical Description of MODEL 931 ECAT SCANNER, Computer Technology & Imaging, Inc., Knoxville TN, May 1986.
17) Jones W. F., Casey M. E., Byars L. G. and Burgiss S. G., IEEE Transactions on Nuclear Science **33** (1986) 601.

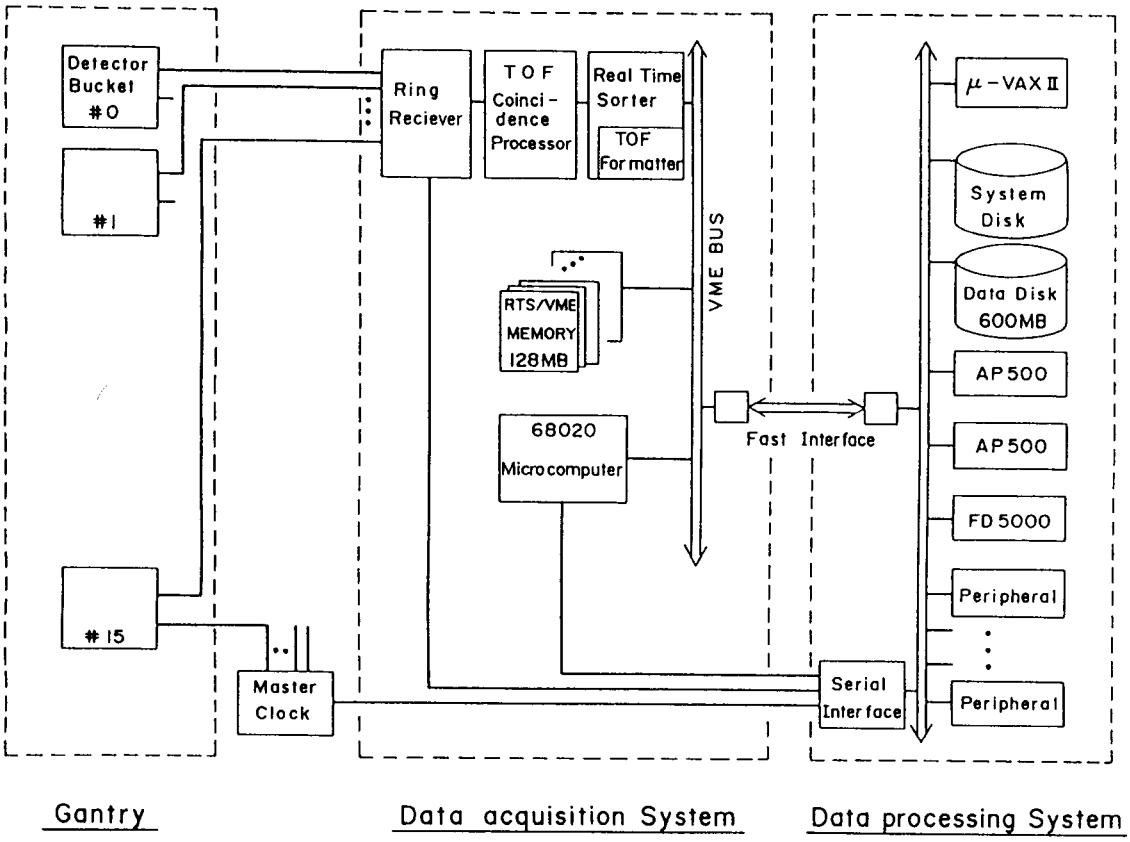

Fig. 1. Block diagram of the TOF-PET.

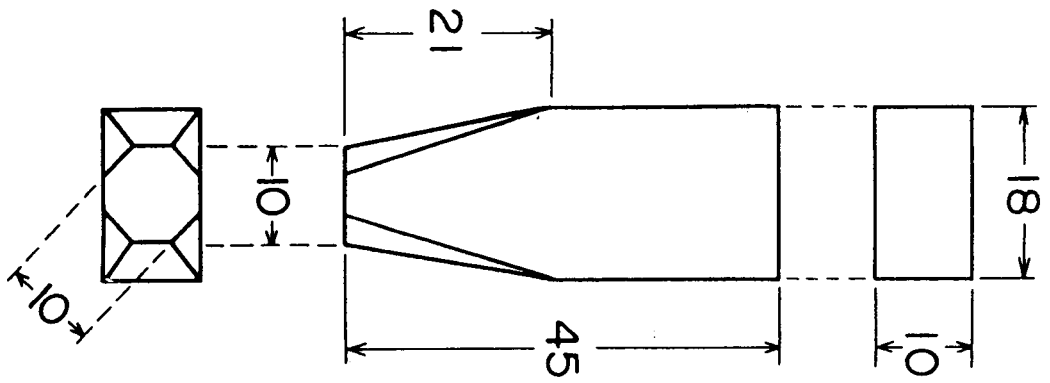

Fig. 2. Design of BaF_2 crystal. The crystal is a dodecahedron of which surfaces are well polished.

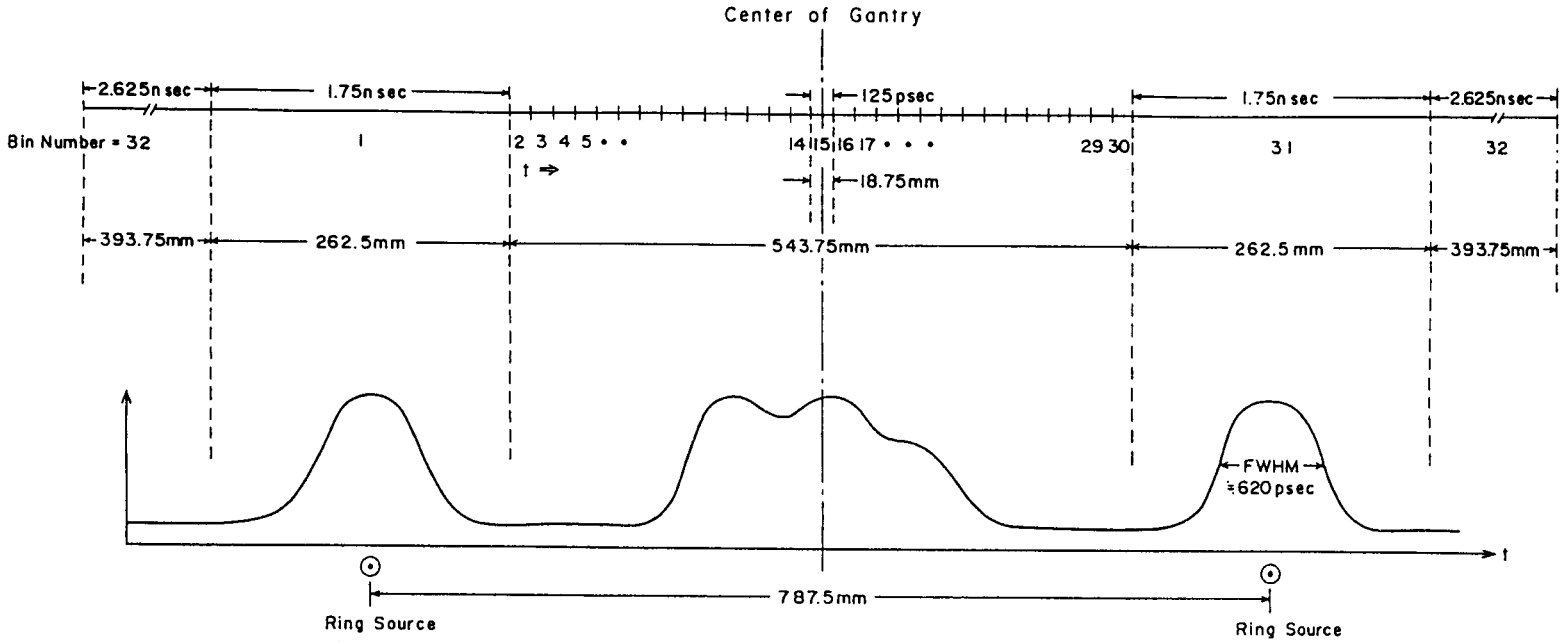

Fig. 3. Time data structure. The present system has 32 bins for storing time data. Bins No. 2-30 are used to the TOF sinogram, those of No. 1 and 31 for a ring source and No. 32 for random coincidence events.

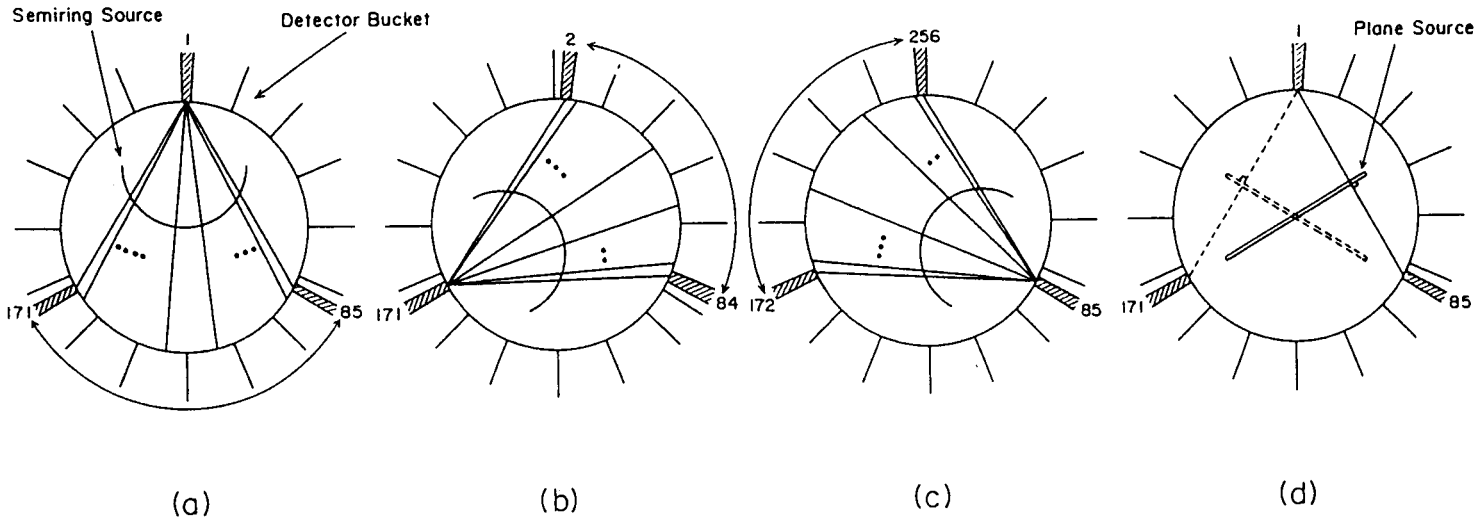

Fig. 4. Time alignment routine. Using a semiring source, all detectors can align their time axes with that of the detector 1 by the process of (a) → (b) → (c). A more accurate alignment of reference detectors of No. 171 in (b) and No. 85 in (c) is achieved with a plane source in (d).

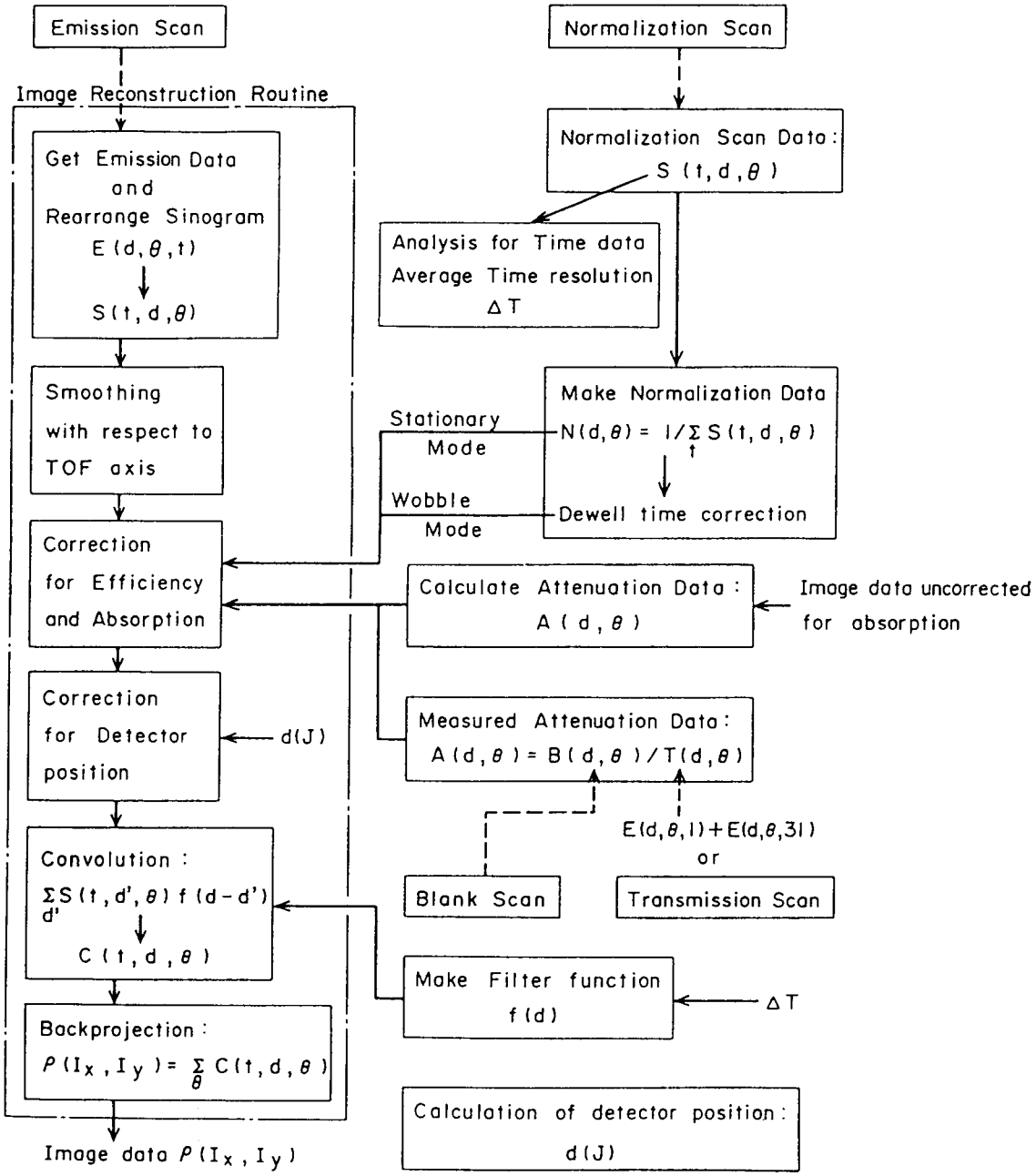

Fig. 5. Flow chart of the image reconstruction programs.

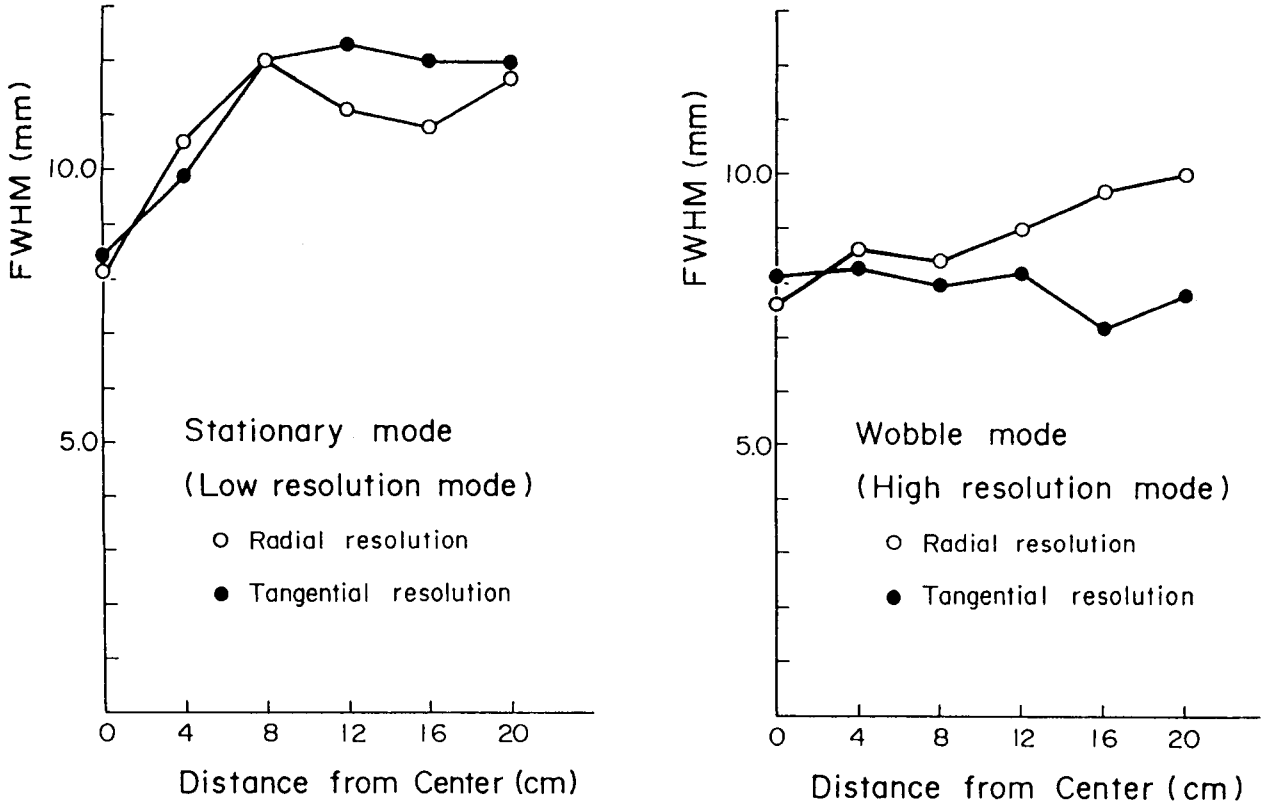

Fig. 6. Spatial resolution of TOF-PET as a function of distance from the center of gantry.

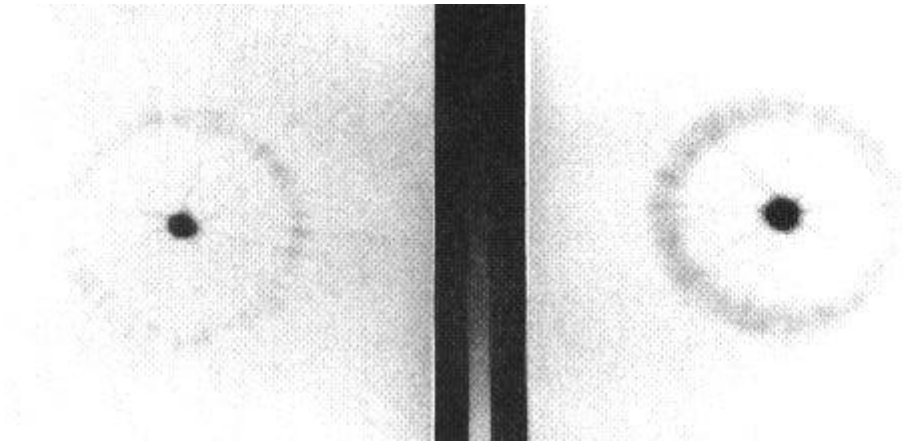

Fig. 7. Examination of image quality with a cylindrical phantom divided into three layers. NON-TOF and TOF show the images reconstructed without and with the use of TOF informations respectively.

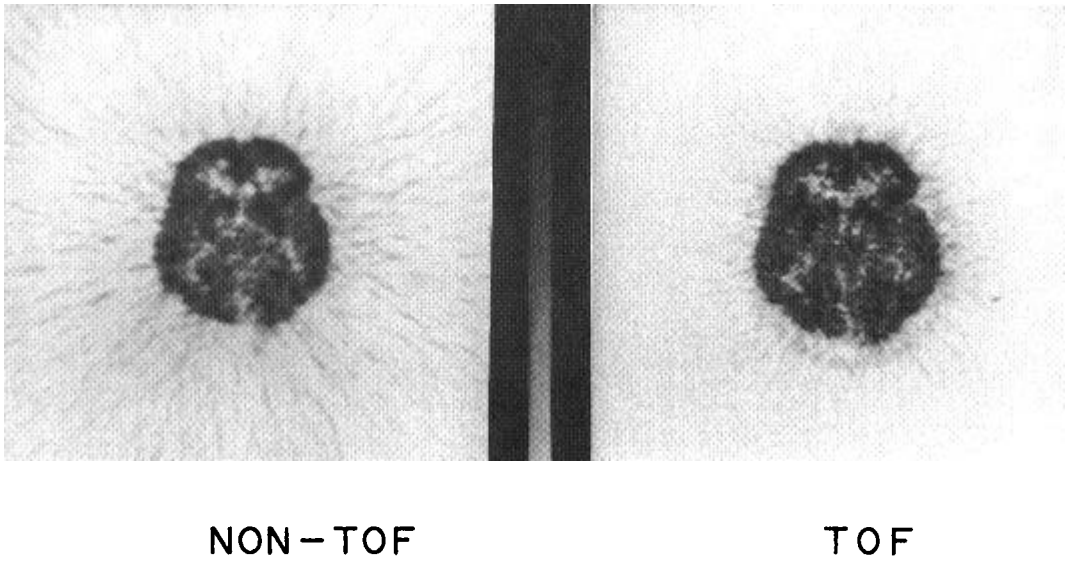

Fig. 8. Effect of using TOF informations in an example of human brain.